CrossMark

Giant dielectric response and magnetoelectric behavior of 95BiFeO₃–5BaTiO₃ (95BFO–5BT) ceramics

Rajesh R. Raut[1] · Paresh H. Salame[2,3] · Jayant T. Kolte[3] · Chandrakant S. Ulhe[4] · Prakash Gopalan[3]

Abstract A detailed study of electrical behavior of 95BiFeO₃–5BaTiO₃ (95BFO–5BT) ceramics through comprehensive analysis of temperature and frequency dependent dielectric behavior, ac impedance and magnetodielectric (MD) properties is reported here. Addition of insulating BaTiO₃ into BiFeO₃ have exhibited enhanced dielectric and ferromagnetic responses. The remnant polarization (P_r) was found to be 6 μC/cm^2, while the dielectric constant was found to be very high ($\varepsilon'_r \geq 10^2$, for T $\geq$ 140 °C). Along with strong conductivity contribution to ε'_r, spectroscopic plots of ε'_r revealed the Maxwell–Wagner type relaxation in the sample, which ultimately could have led to an apparent high ε'_r in 95BFO–5BT ceramics. Origin of such a high ε'_r in BFO–BT was further investigated using impedance spectroscopy. MD studies revealed the magneto-electric coupling in the ceramics. The MD studies along with anomaly in dielectric data near antiferromagnetic ordering temperature ($T_N = 170$ °C) of BFO suggests the magnetic bearing on the electrical properties of 95BFO–5BT ceramics.

✉ Paresh H. Salame
paresh.salame@gmail.com

✉ Jayant T. Kolte
jayantkolte@iitb.ac.in

[1] Department of Physics, Sanmati Engineering College, SGB Amravati University, Amravati, India

[2] Department of Applied Physics, Laxminarayan Institute of Technology, RTM Nagpur University, Nagpur, India

[3] Department of Metallurgical Engineering and Materials Science, Indian Institute of Technology Bombay, Powai, Mumbai 400076, India

[4] Department of Physics, Yashvantrao Chavan Arts and Science College, SGB Amravati University, Amravati, India

1 Introduction

Materials exhibiting two or more coupled functional properties have gained much attention during the last two decades due to their potential applications in advanced technologies. Multiferroic materials simultaneously exhibit multiple ferroic properties, such as ferroelectricity, ferroelasticity, and ferromagnetism (or antiferromagnetism). These multiferroic materials have been used in the magnetic data storage devices, sensors, transducers, etc. [1–6]. Amongst the materials exhibiting multiferroic properties, BiFeO₃ (BFO) has emerged as one of the most extensively investigated multiferroic material, which have shown multiferroic behaviour at room temperature. BFO is ferroelectric with a Curie temperature (T_C) of about 830 °C and antiferromagnetic with a Neel temperature (T_N) at around 370 °C [7, 8].

BiFeO₃, a semiconducting material, forms a solid solution with BaTiO₃ (BT), which is insulating in nature, the small addition of BT into BFO have resulted in enhancing the overall electrical properties. This have also resulted in stabilizing the perovskite structure, as both the materials have perovskite (ABO₃) structure [9–16]. In this paper, BT has been chosen to form solid solution with BFO, owing to its excellent ferroelectric properties (for single crystal, $T_C = 120$ °C, $P_S = 26$ μC/cm^2 and $\varepsilon'_r = 2000$, and for polycrystalline, $T_C = 130$ °C, $P_S = 14.6$ μC/cm^2, and $\varepsilon'_r = 1400$–2100) [17, 18]. Considering these useful electrical properties exhibited separately by BFO and BT, BFO–BT in solid solution/composite form has been widely studied for improvement in the dielectric, multiferroic, piezoelectric properties of pure BFO [9–16].

Along with the interesting electrical properties, the structural properties of BFO–BT solid solution are also fascinating. With earlier investigations on BFO–BT

ceramics verifying that, for BFO content above 70 mol% the structure is rhombohedral while below 4 mol%, it is tetragonal and in between these composition range, the structure is cubic [9, 19]. These structural changes have resulted in exhibiting anomalies in the dielectric and magnetic susceptibility behavior [9]. These anomalies have led to infer that there is a close relationship between structural change and the dielectric/magnetic properties of $(1 - x)BFO–(x)BT$ [20–22].

In this paper, we discuss the results on structural, electrical, magnetic, magnetodielectric (MD), magnetoelectric (ME) properties of $95BiFeO_3–5BaTiO_3$ (95BFO–5BT) ceramics. Emphasis is given to the impedance spectroscopy (IS) analysis of this compound, to find the effect of grain and grain boundary contribution on the electrical properties and to find the origin of high dielectric constant in this ceramics using dielectric spectroscopic plots and IS.

2 Experimental

For Synthesis of 95BFO–5BT ceramics, first, nano-crystalline, single phase BFO powder was prepared by PVA sol–gel method, reported elsewhere [23]. A ceramics of 95BFO–5BT was prepared by mixing $BaTiO_3$ (Sigma-Aldrich, purity >99.9 %) with BFO in a proportionate amount using agate mortar and pestle. This mixed powder was then ball milled for 24 h to get homogeneous fine mixture. Subsequently, the powder was compressed into green pellets using uniaxial hydraulic press and sintered at 870 °C/4 h. These sintered pellets were characterized for their structural properties using a powder X-ray diffraction (PANalytical X'pert Pro). Surface morphology was investigated using scanning electron microscope (SEM) (Jeol JSM-7600F). Dielectric and impedance measurements were carried out by using Novocontrol broadband dielectric spectrometer (Alpha A analyzer Novocontrol GmbH, with BDS 1200 sample holder), in the frequency range of 1 Hz to 1 MHz and temperature range of 0–350 °C. Magnetodielectric measurements were carried using a sample holder placed in between the DC magnets. The ferroelectric properties were investigated using hysteresis loop tracer (TF 2000E, aixACCT GmbH) at 10 Hz. Magnetic characterization was performed on 50 mg of 95BFO–5BT powder using quartz sample holder in vibrating sample magnetometer (Quantum Design, USA).

3 Results and discussion

3.1 Phase detection and microstructure analysis of 95BFO–5BT ceramics

Figure 1 shows the powder XRD pattern of 95BFO–5BT ceramics sintered at 870 °C. The XRD pattern shows that

the addition of BT to BFO has altered the crystal structure of the BFO into a distorted rhombohedral system, which is also shown in figure. The crystal structure of the BFO ceramics and the 95BFO–5BT exhibited pure perovskite structure without any frequently observed secondary phases viz. $Bi_2Fe_4O_9$ and $Bi_{25}Fe_4O_{39}$, while synthesizing BFO and 95BFO–5BT ceramics. The diffraction pattern of this ceramics matches very well with a single phase BFO, which belongs to R3c space group ($a = b = 5.5876$ Å, $c = 13.8670$ Å). Further, it can be confirmed from the XRD figure that $BaTiO_3$ with 5 wt% mixing with $BiFeO_3$ has resulted in forming a solid solution, as no signature of $BaTiO_3$ is visible from XRD pattern.

The SEM photomicrograph of pure BFO and 95BFO–5BT ceramics sintered at 870 °C is shown in Fig. 2. The 95BFO–5BT sample revealed a dense microstructure with rectangular grain morphology and uniform grain size distribution. The average grain size of the 95BFO–5BT sample was found to be around 0.5 μm. Further, it was observed that the addition of BT into BFO has resulted in improving the density as compared to BFO, with sintered BFO showing more porosity than the 95BFO–5BT ceramics. It is thus inferred that $BaTiO_3$ addition has resulted in the formation of more uniform grains in the ceramic matrix, most likely due to the A- and B-site replacements with Ba^{2+} and Ti^{4+} and in the ABO_3 perovskite structure.

3.2 Dielectric behavior of 95BFO–5BT ceramics

In this section, we report the dielectric properties of 95BFO–5BT ceramics in a broad frequency (1 Hz–1 MHz) and temperature (0–350 °C) ranges. Further, the conductivity contribution as well as the effect of Maxwell–Wagner relaxation in dielectric spectra is explored here.
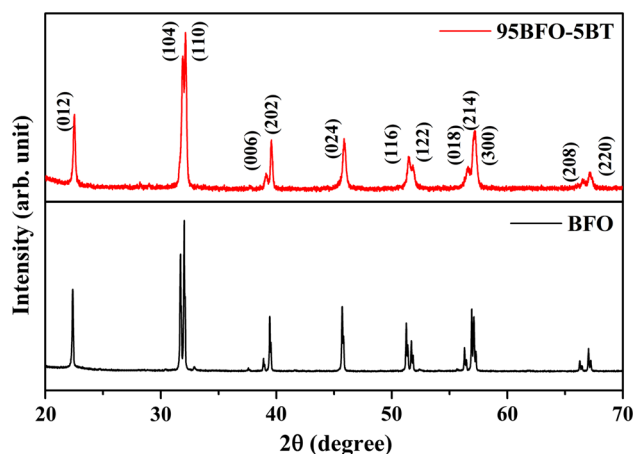

Fig. 1 Powder X-ray diffraction pattern of pure BFO and 95BFO–5BT ceramics, revealing phase purity with no secondary phases
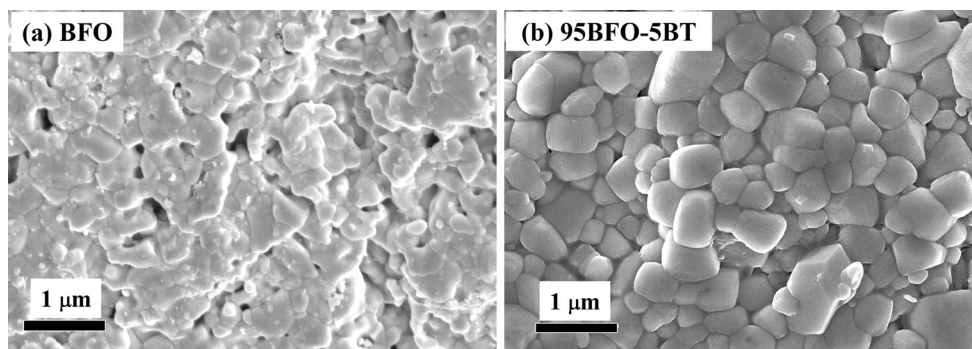
Fig. 2 Scanning electron photomicrograph of pure BFO and 95BFO–5BT ceramic sintered at 870 °C

3.2.1 Temperature dependence of ε_r' for 95BFO–5BT ceramics

For the 95BFO–5BT ceramics, the temperature (0–350 °C) dependence of relative permittivity (ε_r) and dielectric loss (tan δ) at a few selected test frequencies is shown in Fig. 3. A very high dielectric constant ($\varepsilon_r' > 10^2$–10^3, especially for $f < 100$ kHz) and low loss (tan δ ≤ 1) are observed over the entire measured temperature ranges for the sample. Further, this dielectric behavior have shown a characteristic step-like decrease in ε_r', which becomes almost temperature independent for $f < 10$ kHz and T < 150 °C. Furthermore, with an increase in temperature a broad relaxation peak (in tan δ) is observed accompanying ε_r' at around 150–225 °C. This relaxation in ε_r' is interestingly close to the magnetic transition temperature of BFO, indicating the magnetic-electric coupling of 95BFO–5BT. These loss peaks can be seen shifting towards higher temperatures with the increase in frequency indicating the relaxation process is thermally activated. In addition to this relaxation phenomenon, there is always a likelihood of simultaneous presence of Fe^{2+} and Fe^{3+} valence state in
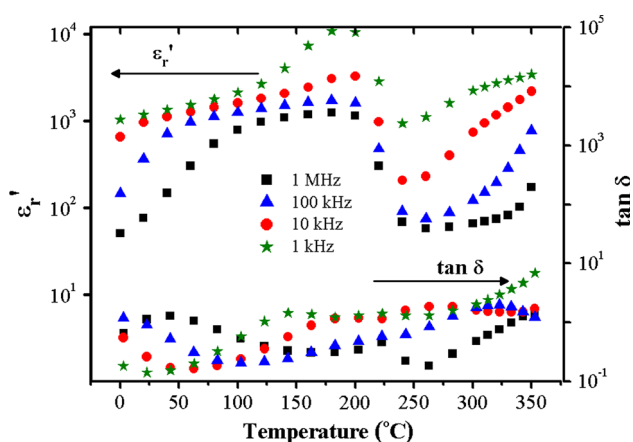
$BiFeO_3$. The hopping of electrons back and forth between these two valence states could lead to dipolar polarization and may also enhance the dielectric permittivity. As a consequence, both kinds of the mechanism viz. proximity to T_N and presence of two valence states, as mentioned above could cooperatively lead to the occurrence of dielectric relaxation peaks.

3.2.2 Frequency dependence of the dielectric constant of 95BFO–5BT ceramics

As discussed in previous section, the temperature dependent dielectric behavior revealed very high values of dielectric constant ($\varepsilon' \geq 100$). The origin of such a high ε' with added BT can be explained by the spectroscopic plots of ε_r', wherein a clear Maxwell–Wagner type of relaxation is seen (see Fig. 4a). Figure 4a shows the dielectric (ε_r') dispersion of 95BFO–5BT ceramics with frequency. High values of $\varepsilon_r' > 10^2$ for $T > R_T$, were revealed by the 95BFO–5BT. Effect of space charge polarization, contributing to $\varepsilon_r' > 10^3$ can be seen at lower frequencies (<100 Hz). However, this space charge polarization effect does not sustain at higher frequencies (>100 Hz) and a gradual decrease in ε_r', due to inability of dipoles created at interfaces to align themselves to the applied frequencies, is observed with the frequency. Hence, a continuous decrease in the ε_r' with frequency is seen here. Further, a step-like decrease in ε_r' is observed which can be seen shifting towards the higher frequency side. This sudden fall in ε_r' is again followed by the frequency stable, plateau-like region in ε_r'. Corresponding to this step-like fall in ε_r', there is a peak in the ε_r'' versus f plot (see Fig. 4b). This feature is the typical of the Maxwell–Wagner type relaxation process in the sample. These peaks can also be seen shifting towards higher frequencies with the increase in temperature as observed in ε_r'.

Further, from Fig. 4b ε_r'' can be seen varying with slope of ~ -1 prior to the inflection point of the relaxation peak. This variation of $\Delta\varepsilon_r''/\Delta f$ with slope of -1 signifies that the
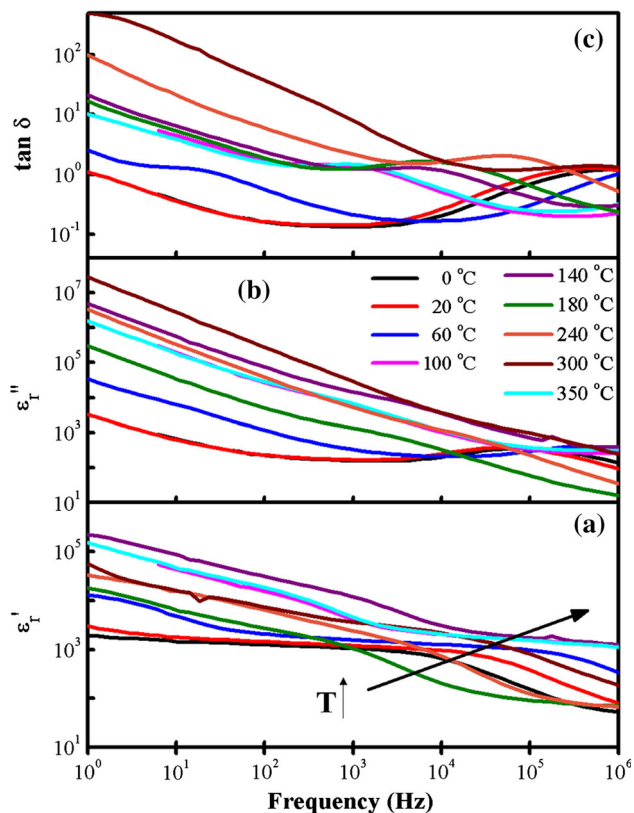

Fig. 3 Real part of dielectric constant (ε_r') and dielectric loss (tan δ) as a function of temperature for 95BFO–5BT ceramics

Fig. 4 Variation of **a** real part ε_r', **b** imaginary part ε_r'' and **c** dissipation factor tan δ, of the dielectric constant

dc conductivity ought to be a prime contributor to the dielectric losses in the sample. This conductivity contribution to the dielectric losses in the sample can be represented by [24]

$$\varepsilon_r'' = \sigma_{dc}/\omega\varepsilon_o \qquad (1)$$

where, σ_{dc} is the dc conductivity contributed through the leakage current in the sample and ε_o is the permittivity of free space.

Figure 4c shows the variation of dissipation factor (tan δ) with frequency, a similar kind of Maxwell–Wagner relaxation process is also seen from the spectroscopic plot of tan δ, wherein strong relaxation peaks can be seen shifting towards higher frequency side with an increase in temperature. Moreover, it can also be infer that the high dielectric loss (tan δ) observed in 95BFO–5BT ceramics is most likely due to the hopping of charge carrier between Fe^{3+} and Fe^{2+} valence state. This dominant factor clearly controls the observed dielectric characteristics of the sample, rather than the highly insulating behaviour of the BT constituent [25].

The display of strong increase in the real part of permittivity to such high values ($\sim 10^4$) and tan δ above unity with increasing temperature (particularly at lower

frequencies) indicates important contributions from conductivity relaxation combined with Maxwell–Wagner phenomena to the total dielectric response.

3.3 AC conductivity behavior of 95BFO–5BT ceramics

Figure 5 shows the variation of AC conductivity (σ_{ac}) plotted as a function of frequency at few selected temperatures (0–350 °C). It is observed that the spectrum exhibits two different regions. At low to intermediate frequencies, a plateau in the spectrum, which usually corresponds to the dc conduction (σ_{dc}) in the sample, is seen. Further, this flattened region becomes wider and is seen shifting toward higher frequencies with increasing temperature which suggest the formation of conducting path throughout the materials. With the increase in frequency, a dispersion in the AC conductivity is observed with the increase in conductivity. This is known to be a typical conduction mechanism observed in ceramic assisted by the polaronic hopping between the available states. Jonscher's power law can describe such frequency dispersion in AC conductivity due to polaronic hopping [26], given by;

$$\sigma_{ac} = \sigma_o + A\omega^n, \qquad (2)$$

where, A is a material specific constant, σ_o is the extrapolated dc conductivity and n is the temperature dependent exponent. Jonscher's power law can be seen best fit with the experimental data (see Fig. 5), the value of n and dc conductivity were calculated from the fitted data using Jonscher's power law (the solid lines in the graph indicates the fitted data). The value of n was found to vary between 0 and 1, such values are usually attributed to the conduction due to the translational (i.e. long range) hopping of charge
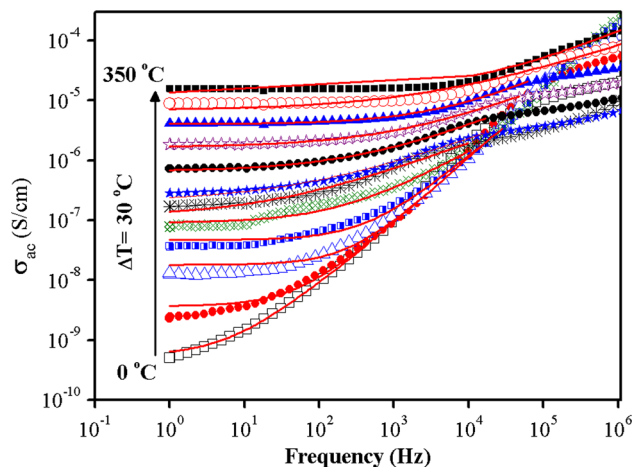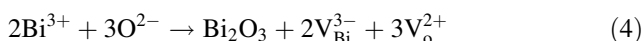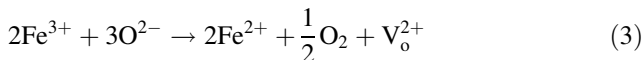

Fig. 5 Variation of ac conductivity (σ_{ac}) with frequency at few discrete temperature, the *solid lines* shows the Jonscher's power law fitted to the experimental data

carriers. Further, with the increase in temperature the conductivity of these samples were found to be increased, probably due to the increase in mobility of oxygen vacancy, and the flattened region shifts upwards and dominates over a larger range of frequencies [27, 28].

In BFO–BT ceramics, in all probability, it is likely that the overall AC conductivity of BFO–BT could arise due to the hopping of oxygen vacancies between the multivalent oxidation states of Fe^{3+} and F^{2+} ions and the presence of bismuth vacancies (V_{Bi}^{3+}) and oxygen vacancies (V_o^{2+}) due to the volatilization of Bi_2O_3 [29]. The reaction in the Kroger–Vink notation can be written as

$$2Fe^{3+} + 3O^{2-} \rightarrow 2Fe^{2+} + \frac{1}{2}O_2 + V_o^{2+} \tag{3}$$

$$2Bi^{3+} + 3O^{2-} \rightarrow Bi_2O_3 + 2V_{Bi}^{3-} + 3V_o^{2+} \tag{4}$$

It is also found that the overall conductivity of the 95BFO–5BT samples has been decreased at least by an order when compared to the BFO samples at various temperatures, suggesting the samples becomes more insulating with the addition of BT.

The dc conductivity (σ_{dc}) calculated from fitting the Jonscher's power law to the experimental data was then used to calculate the activation energy of the conduction of 95BFO–5BT ceramics by using Arrhenius plot. Figure 6 shows an Arrhenius plot (ln σ_{dc} vs. 1000/T) for the estimation of the activation energy. The activation energy was calculated using the Arrhenius equation

$$\sigma_{dc} = \sigma_o \exp(-E_a/K_BT) \tag{5}$$

where, σ_o is the pre-exponential factor, K_B is the Boltzmann's constant and E_a is the electrical activation energy of the conduction. The activation energy (E_a) calculated from the Arrhenius plot revealed two values of activation energies corresponding to two different regions with
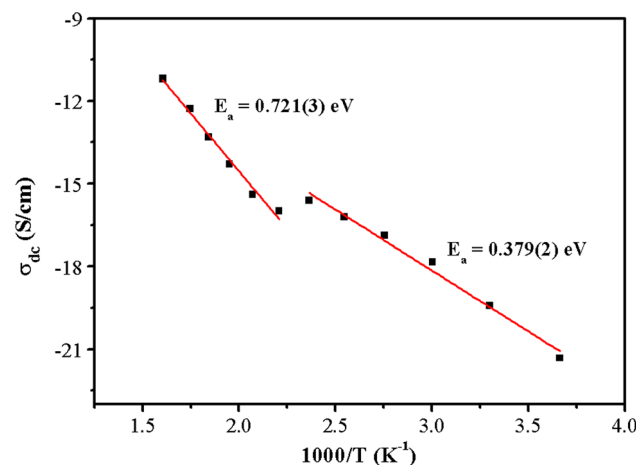
$E_a = 0.721$ eV (for T > 170 °C) and $E_a = 0.379$ eV (for T < 170 °C).

3.4 Complex impedance studies of 95BFO–5BT ceramics

Polycrystalline materials consists of grains and grain boundaries whose capacitive effects have a profound impact on the ferroelectric properties. Impedance analysis is a valuable tool to separate capacitive and resistive contributions arising from grains, grain-boundaries and electrode-specimen interface. The individual contribution from each of these entities can be represented by equivalent parallel RC circuits connected in series. Each RC element of the equivalent circuit give rise to a semicircle with its center lying on the real axis, if there is a single value of relaxation time, τ given by $\tau = 1/\omega$, where ω is the angular frequency corresponding to maxima in $-Z''$ versus Z' plot [9]. However, in physical ceramics, there can be two or more relaxations arising due to contribution of grains, grain boundaries etc.

Figure 7 shows the complex impedance plots for 95BFO–5BT at a few discrete sample temperatures (100–330 °C). The plots show two semicircles, whose centers lay somewhat below the real Z axis, indicating the non-ideal Debye, thereby suggesting the presence of two or more relaxation times. The experimental data was fitted successfully employing equivalent model of the two parallel RC circuits connected in series (the schematic is shown inside the figure). The first semicircle at high frequencies could be due to the contribution of grains to the electrical resistivity and the other at lower frequencies could be due to the contribution of grain boundaries.
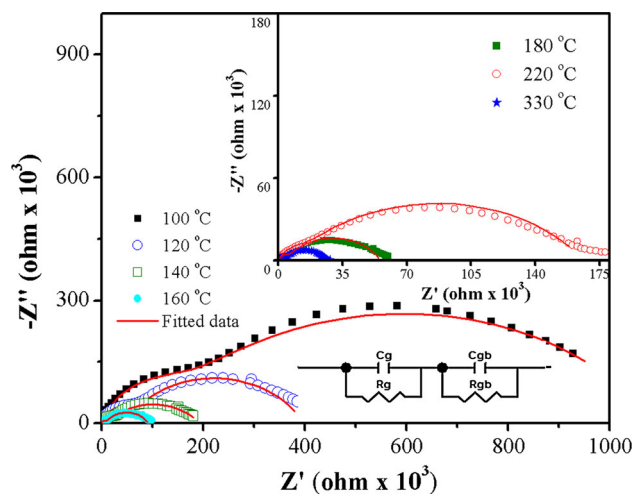

Fig. 6 Arrhenius plot for estimation for activation energy of conduction for 95BFO–5BT ceramics

Fig. 7 Cole–Cole plot for 95BFO–5BT ceramics, showing non-ideal Debye like behaviour. The data is fitted using two parallel RC circuits connected in series, the schematic is shown inside the figure
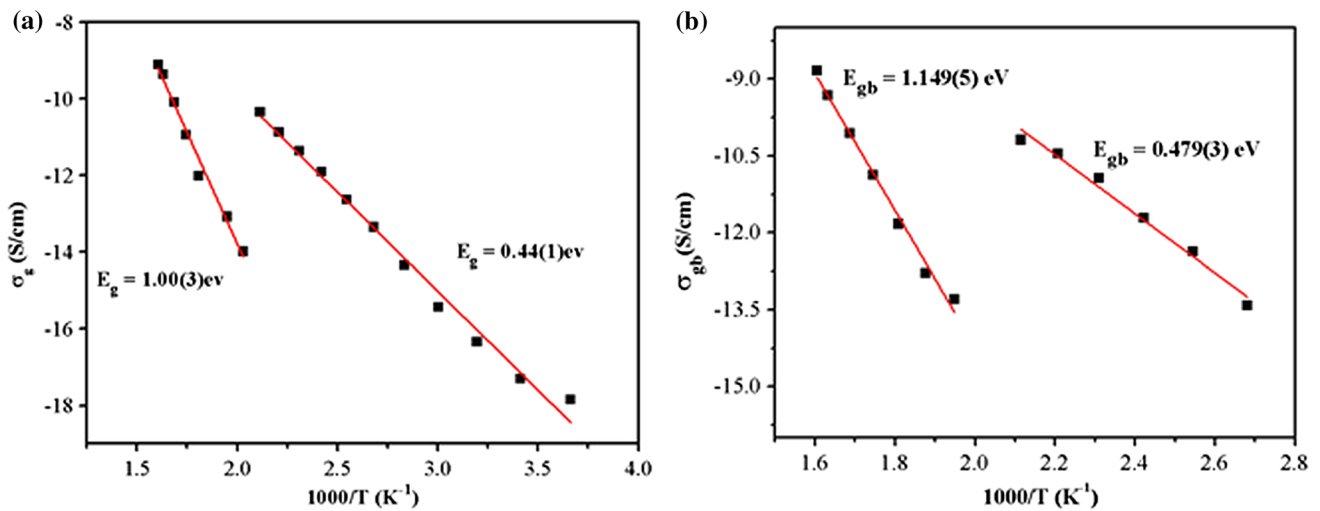
(a)

(b)

Fig. 8 Estimation of activation energy of grain and grain boundary conduction deduced from the Arrhenius plot for the 95BFO–5BT ceramics
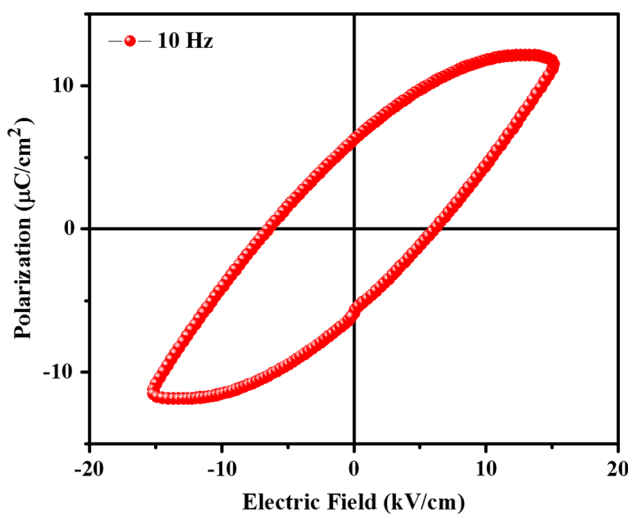

Fig. 9 Ferroelectric hysteresis (P–E) loop for 95BFO–5BT ceramics
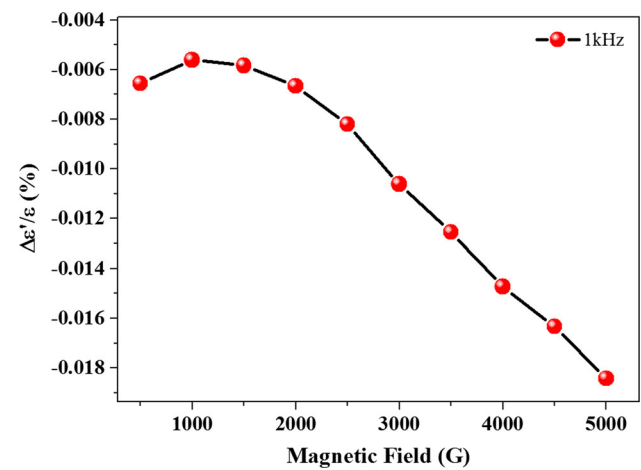

Fig. 10 Magnetodielectric (MD) coefficient of 95BFO–5BT ceramics, measured at room temperature

Similarly, the first RC element represents the contribution of the grain while the second RC circuit represents the contribution from the grain boundaries to the overall impedance.

The values of R_g, R_{gb}, C_g and C_{gb} were estimated from fitting the experimental data to an equivalent series combination of two parallel RC circuits. As shown in Fig. 7, the data is fitted quite accurately using this equivalent circuit model. The values of C_g were found between 10^{-10} and 10^{-11} F, while the C_{gb} values were found to vary between 10^{-8} and 10^{-9} F. The value of R_{gb} was found to be ($\geq 10^4\ \Omega$) which is only 1–2 orders higher than the grain resistance, R_g ($\leq 10^3\ \Omega$). Usually the network of insulating grain boundaries and semiconducting grains could give rise to the internal barrier layer capacitance (IBLC) effect, as observed in many high dielectric and high loss oxide

electro-ceramics [24, 29, 30]. However, in this sample the difference in grain and grain boundary resistance is not that much. It is inferred that the sample is electrical homogeneous.

Thus, IBLC effect, as observed in other high dielectric constant oxide material is not contributory in this 95BFO–5BT ceramics. And, Maxwell–Wagner response, as observed from the dielectric spectra as well as hopping of charge carriers between two different valence states of Fe can only be held responsible for apparent high dielectric constant in 95BFO–5BT ceramics.

Further, these impedance plots were used to calculate the activation energies of grain and grain boundary conduction by knowing the values of R_g and R_{gb} at various temperatures, and taking these values in the Arrhenius plot. The activation energies of the grain and grain boundary
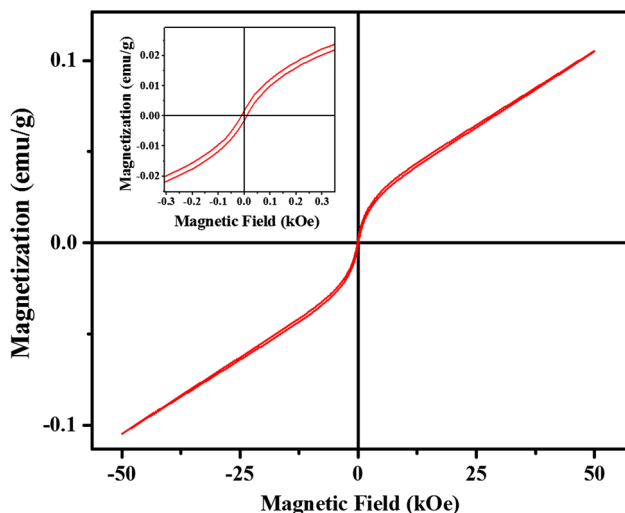
Fig. 11 Magnetic hysteresis loop at room temperature for 95BFO–5BT ceramics

were calculated using the Arrhenius equation (Eq. 5). The values of activation energy for grains (E_g) was found to be 1 eV for T > 170 °C while, for T < 170 °C, the E_g was found to be 0.44 eV. Similarly the activation energy for grain boundary (E_{gb}) conduction was found to be 1.149 eV for T > 170 °C while, for T < 170 °C, it was found to be 0.479 eV (Fig. 8).

3.5 Ferroelectric response of 95BFO–5BT ceramics

Electric hysteresis loop of 95BFO–5BT measured at 100 Hz and room temperature is shown in Fig. 9. The sample shows ferroelectric (P–E) hysteresis loops at an applied field of 10–20 kV/cm. Addition of BT altered the P versus E hysteresis loop of 95BFO–5BT. The sample exhibited maximum polarization of about 11 μC/cm^2. The remnant polarization (P_r) and coercive field (E_c) was noted approximately to be 6 μC/cm^2 and 6.28 kV/cm, respectively. The incorporation of BT into BFO could probably result in substituting Ti^{4+} for Fe^{3+} in BFO thus compensating the electron deficiency, thereby reducing the leakage current and improving the overall electrical properties.

3.6 Magneto-dielectric properties of 95BFO–5BT ceramics

To study the magneto-electric (ME) coupling in the present BFO–BT ceramics, magnetic field dependence of dielectric constant (ε'_r), also called as magneto-dielectric (MD) coefficient is measured at 1 kHz applied frequency to the sample using the following equation [31],

$$\text{MD} \% = \frac{\varepsilon'_r(H) - \varepsilon'_r(0)}{\varepsilon'_r(0)} \times 100 \qquad (6)$$

where, $\varepsilon'_r(H)$ and $\varepsilon'_r(0)$ are dielectric constants at applied field and zero field. The field dependence of MD effect was calculated and is shown in Fig. 10. The field dependence of MD effect is milder in BFO–BT ceramics as compared to the pristine BFO, probably due to the fact that BT not being multiferroic in nature. It can be clearly seen from the figure that the MD coefficient has increased from 0.006 at 0 Gauss to 0.018 at 5 kG with the magnetic field.

3.7 Magnetic properties of 95BFO–5BT ceramics

The magnetic hysteresis loops for 95BFO–5BT sample at room temperature is shown in Fig. 11. The substituting Ba and Ti ions broke the incommensurate cycloid spin structure of the BFO, leading to a canted structure due to the Dzyaloshinskii–Moriya interaction [32] resulting in weak ferromagnetism, which is considerable in the 95BFO–5BT sample. For small BT concentrations in the BFO–BT system, the charge balance implies the formation of few oxygen vacancies and, consequently, few Fe^{2+} or Ti^{3+} ions in the perovskite unit cell. Recent discussion on magnetism in pure $BaTiO_3$ proposed that the partially filled Ti orbital and the partially polarized O $2p$ electrons for the Ti and O vacancies are responsible for magnetism [33]. The saturation magnetization value for 95BFO–5BT was found to be 0.1 emu/g at the applied magnetic field of 50 kOe.

4 Conclusions

In the present work, highly insulating 95BFO–5BT ceramics were synthesized by Sol–Gel ($BiFeO_3$) followed by mixing (with $BaTiO_3$) method. XRD confirms the distorted rhombohedral phase of sample sintered at 870 °C/24 h in air. Extremely high values ($\varepsilon'_r > 10^3$, especially for $f < 100$ kHz) and low loss (tan δ ≤ 1) were observed for the entire measured temperature ranges for the sample. Electrical homogeneity of microstructure of 95BFO–5BT ceramics was revealed using IS, which ruled out the applicability of the IBLC effect, as observed for other high dielectric constant, high loss oxide materials. Instead, in all probability the origin of high dielectric constant could be attributed to the Maxwell–Wagner response and hopping of charge carriers between +2 and +3 valence states of Fe. AC conductivity of the 95BFO–5BT samples is found to be decreased, suggesting the sample becomes more insulating with the addition of ferroelectric BT. The MD dependence of the 95BFO–5BT showed a milder effect of magnetic field on electric polarization when compared to the reported values on pristine BFO. However, the addition of BT into BFO have resulted in reducing the dielectric losses and

conductivity of the sample, which is technologically important.

References

1. N.D. Mathur, W. Eerenstein, J.F. Scott, Nature **442**, 759 (2006)
2. M. Fiebig, J. Phys. D Appl. Phys. **38**, R123 (2005)
3. I. Sosnowska, T.P. Neumaier, E. Steichele, J. Phys. C **15**, 4835 (1982)
4. G.D. Achenbach, W.J. James, R. Gerson, J. Am. Ceram. Soc. **50**, 437 (1967)
5. C. Tabares Munoz, J.-P. Rivera, A. Bezinges, A. Monnier, H. Schmid, Jpn. J. Appl. Phys. **24**, 1051 (1985)
6. V.R. Palkar, J. John, R. Pinto, Appl. Phys. Lett. **80**, 1628 (2002)
7. S.V. Kiselev, R.P. Ozerov, G.S. Zhdanov, Sov. Phys. Dokl. **7**, 742 (1963)
8. P. Fischer, M. Polomska, I. Sosnowska, M. Szymanski, J. Phys. C **13**, 1931 (1980)
9. M.M. Kumar, A. Srinivas, S.V. Suryanarayana, J. Appl. Phys. **87**, 855 (2000)
10. M.T. Buscaglia, L. Mitoseriu, V. Buscaglia, I. Pallecchi, M. Viviani, P. Nanni, A.S. Siri, J. Eur. Ceram. Soc. **26**, 3027 (2006)
11. R. Rai, I. Bdikin, M.A. Valente, A.L. Kholkin, Mater. Chem. Phys. **119**, 539 (2010)
12. R.A.M. Gotardo, I.A. Santos, L.F. Cótica, É.R. Botero, D. Garcia, J.A. Eiras, Scr. Mater. **61**, 508 (2009)
13. S.O. Leontsev, R.E. Eitel, J. Am. Ceram. Soc. **92**, 2957 (2009)
14. C. Zhou, H. Yang, Q. Zhou, G. Chen, W. Li, H. Wang, J. Mater. Sci.: Mater. Electron. **24**, 1685 (2013)
15. H.Y. Dai, J. Chen, T. Li, D.W. Liu, R.Z. Xue, H.W. Xiang, Z.P. Chen, J. Mater. Sci.: Mater. Electron. **26**, 3717 (2015)
16. M. Kumar, S. Shankar, O. Thakur, A. Ghosh, J. Mater. Sci.: Mater. Electron. **26**, 1427 (2015)
17. J. Bernard, *Piezoelectric Ceramics* (Academic Press, New York, 1971)
18. G. Arlt, D. Hennings, G. de With, J. Appl. Phys. **58**, 1619 (1985)
19. Y. Yuan, M. Du, S. Zhang, Z. Pei, J. Mater. Sci.: Mater. Electron. **20**, 157 (2009)
20. W. Li, J. Qi, Y. Wang, L. Li, Z. Gui, Mater. Lett. **57**, 1 (2002)
21. A. Umeri, T. Kuku, N. Scuor, V. Sergo, J. Mater. Sci. **43**, 922 (2008)
22. Y. Yuan, S. Zhang, W. You, Mater. Lett. **58**, 1959 (2004)
23. J. Kolte, D. Gulwade, A. Daryapurkar, P. Gopalan, Mater. Sci. Forum **702**, 1011 (2012)
24. P. Salame, R. Drai, O. Prakash, A.R. Kulkarni, Ceram. Int. **40**, 4491 (2014)
25. S. Chandarak, A. Ngamjarurojana, S. Srilomsak, P. Laoratanakul, S. Rujirawat, R. Yimnirun, Ferroelectrics **410**, 75 (2010)
26. A.K. Jonscher, Nature **267**, 673 (1977)
27. C.R. Bowen, D.P. Almond, Mater. Sci. Technol. **22**, 719 (2006)
28. D.P. Almond, C.R. Bowen, D.A.S. Rees, J. Phys. D Appl. Phys. **39**, 1295 (2006)
29. P.H. Salame, O. Prakash, A.R. Kulkarni, J. Am. Ceram. Soc. **96**, 2184 (2013)
30. T.B. Adams, D.C. Sinclair, A.R. West, Adv. Mater. **14**, 1321 (2002)
31. A. Mukherjee, S. Basu, P.K. Manna, S.M. Yusuf, M. Pal, J. Mater. Chem. C **2**, 5885 (2014)
32. T. Moriya, Phys. Rev. **120**, 91 (1960)
33. D. Cao, M.Q. Cai, Y. Zheng, W.Y. Hu, Phys. Chem. Chem. Phys. **11**, 10934 (2009)